3D printed organ models and patient-specific dosimetry for children with heart disease

Pedro Silva[1,a]

[1] *Instituto Superior Técnico, Lisboa, Portugal*

Abstract.
The interest and use of 3D printing in clinical applications has been steadily advancing in recent years given that this technology has a great capacity to produce increasingly detailed anatomical structures and replicate complex anomalies.
The main goal of this thesis is to create 3D printed models of the hearts of children with heart disease, whether congenital or acquired. Often, paediatric patients with heart disease are subject to different types of radiological examinations throughout their lives. This early and protracted exposure to ionising radiation is a source of concern as exposure may increase lifetime risk for cancer and other diseases.
The models were produced using data from three patients, through Computed Tomographies (CT) and Magnetic Resonances (MRI), at the Centro de Referência de Cardiopatias Congénitas do Hospital de Santa Marta, following national data protection norms and ethical standards.
The printed models showed an adequate quality of segmentation and impression, accurately reproducing the anatomical characteristics of the heart and vasculature. However, the limitations of CT in relation to contrast for different soft tissues and the lower resolution of MRI may cause imperfections located in 3D printed models.
This type of technology is currently not available in the Portuguese health care system. So, by delivering to the medical community a fast method to improve interventional and surgical outcomes, as well as dose optimisation procedures, it will become a clear advantage for the patient's outcome and quality of life.

Keywords: 3D printing, Heart disease, Ionising radiation, Dosimetry.

1 Introduction

1.1 Motivation

In the past years, the use of 3D printing in medicine has been increasing. This technology can create realistic, personalised and anatomically accurate models for niche applications specifically in Cardiology.

Heart disease, whether congenital or acquired, with diverse and sometimes complex pathologies would benefit from this technology by presenting a complete representation of the anatomy, bring out a deeper understanding of complex spatial relationships between different structures and providing a personalised treatment adequate to the patient [1].

Understanding and visualising the surgical anatomy from the images obtained through imaging methods is limited and requires a difficult process of mental reconstruction and can be often inadequate or incomplete [1, 2]. Furthermore, by using a patient-specific anatomical model of the heart, discussions within the medical teams managing complex cases will be facilitated, cardiologists may feel more prepared, and experienced surgeons and interventional radiologists can develop innovative approaches to cases, thus yielding better patient outcomes, lowering intervention time and re-intervention rate [3].

This type of technology can also serve as an educational tool to train students on more complex anatomy and allowing them to explore rare cases with detailed models. In addition, these models will be useful to patients and their families expanding their understanding of their condition and endow them with the necessary information in order to make informed decisions.

[a] e-mail: pedro.freitas.silva@tecnico.ulisboa.pt

3D printed models may as well enable further developments in medical physics such as an accurate effective dose estimation; for instance, the tissue-weight dose quantity, in paediatric patients with heart disease that need diagnostic or interventional procedures that require radiation. Due to their condition, paediatric patients with congenital heart disease (CHD) are subject to various diagnostic X-ray examinations since the early stages of their lives. The optimisation of paediatric patient doses, still remains an unsolved question in diagnostic and interventional radiology [4]. Therefore, to solve this issue, a wide range of dosimetric measurements has to be made from all ages, extending from a neonate to an adult, to ensure that the findings are the most accurate possible.

The main goal is to create 3D printed models of the hearts of children with heart disease. Moreover, these models can be used to estimate the dose received in the CT procedure and eventually contribute to an optimisation of protocols for children from newborn to older ages.

This thesis offers the opportunity to work in a multidisciplinary environment, with physicists, physicians, radiologists among others. It is in the scope of a collaborative project with the group of Professor Matheus Savi of the Instituto Federal de Santa Catarina and the Paediatric Cardiology team of the Centro de Referência de Cardiopatias Congénitas (CRCC) of the Hospital de Santa Marta, Centro Hospitalar Universitário de Lisboa Central (CHULC), Lisboa.

1.2 3D printing

3D printing is a technique that is used to transform digital models into physical models. The technology was first

introduced in 1986 and since then it has grown to encompass different manufacturing technologies for various applications in different areas [2, 5].

The process of 3D printing applied to medicine can be summarised by the acquisition of a imaging data-set through an imaging procedure (figure 1a and 1b); the segmentation of the anatomy using specialised software (figure 1c); design refinement such as the addition of cut-planes and model stability elements using CAD software; the STL file conversion (figure 1c) and finally printing the physical model (figure 1d) [6].

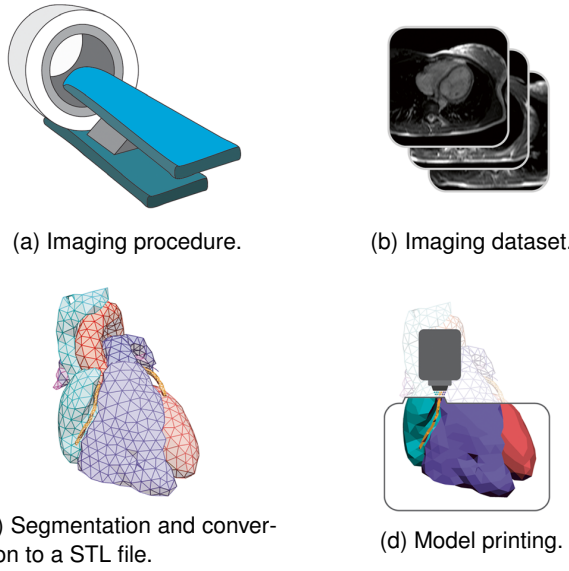

(a) Imaging procedure.

(b) Imaging dataset.

(c) Segmentation and conversion to a STL file.

(d) Model printing.

Figure 1: 3D printing process. Retrieved from [3].

2 Methodology

2.1 Anatomical terminology

In order to provide a comprehensive explanation of the structures and their relative position in the body, some terminology has to be presented particularly directional terms and the body planes.

The directional terms are based on the body being viewed in the anatomic position i.e. from the point of view of the subject, not the observer [7]. The term anterior refers to movement or structure towards the front of the body while posterior regards to movement or structures towards the back of the body. Inferior describes downward movement or describes a position below another part of the body. On the contrary, superior defines upward movement or to classify a position above another part of the body [7].

A body plane represents a section of the body, where a section is a two-dimensional surface of a cut three-dimensional volume (figure 2) [8]. Axial planes are horizontal cross-sectional planes that divide the body into a superior and an inferior section. The sagittal plane splits the body into the left and right sections. Lastly, the coronal plane separates the body into anterior and posterior sections. Oblique planes are sections that lie at an angle to one of the three standard planes [7].

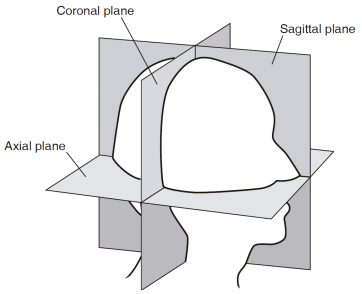

Figure 2: Imaging planes. Retrieved from [7].

2.2 Imaging techniques

The CT data was obtained from a state-of-the-art 128-slice CT scanner SOMATOM Definition Flash (Siemans, Erlangen, Germany) using an iodinated contrast medium at Hospital de Santa Marta, Lisbon. All the data covered the whole heart from the upper abdomen to the aortic arch. The average axial slice thickness is 0.40 mm and the resulting images have a resolution of 512×512 pixels.

The MRI data was acquired by the MRI scanner Optima™ MR450w (GE Healthcare, Chicago, United States of America) being administered a gadolinium contrast medium at Hospital de Santa Marta in Lisbon. The scans covered the whole heart from the upper abdomen to the aortic arch. The average axial slice thickness ranges from 1 mm to 1.2 mm and the resulting images have a resolution of 512×512 pixels.

2.3 Segmentation methodology

The segmentation process allows for the separation of different regions or to delineate boundaries of these regions. The main goal of whole heart segmentation is to extract and separate the desired information like the volume and shapes of the substructures of the heart [9, 10].

Considering we are working with paediatric patients with heart disease, a vast array of dispositions of structures in different subjects exists therefore a fully automatic segmentation is not possible. A semi-automatic method with an image-driven segmentation technique is preferable [11].

The thresholding method may be used to localise and extract a region of interest based on the analysis of the intensity histogram. This method is effective when there is a clear distinction of intensity between the area of interest and the surrounding areas. Occasionally, the intensity of different tissues overlap and the thresholding also encompasses other structures. In these cases, manual editing is necessary to eliminate the selection of non-desired structures in the segmentation [1, 2, 10, 11].

Hence, manual labelling accompanied with the thresholding method was adopted to generate the segmentation. The segmentation was performed by using the open-source software 3DSlicer [12].

The axial, sagittal and coronal view (and sometimes transversal views) were visualised simultaneously in order to easily identify the structures, and to check the consistency, smoothness and to overall aid the segmentation process [13]. After the segmentation is finished and ready to

be printed the software converts and exports the segments into the STL format.

2.4 Printing methodology

In this thesis, two types of printing techniques were used: fused deposition modelling (FDM) and stereolithography (SLA).

FDM is one of the most used 3D printing process due to its high-reliability, low costs and simplicity. The technique is based on the extrusion and then deposition of molten thermoplastic filament onto a platform, fabricating parts layer-by-layer [14]. Most of the segments were printed using this technology with the Pro Core H4 (GTMax3D, São Paulo, Brazil), Ultimaker 3 and Ultimaker 2 Extended+ (Ultimaker, Utrecht, The Netherlands) in combination with ABS filaments (3D.on, Florianópolis, Brazil) and PLA filaments (Alcia 3DP, Spain).

SLA was the first additive manufacturing process to be developed in the 1980s and has withstood the test of time on account of its accuracy, high precision, ability for fine details and its celerity. This procedure works in the layer-by-layer fashion using a guided UV light that leads to the solidification of a liquid resin by photopolymerisation [15]. On the segments that presented intricate and fine details this technique was chosen to manufacture more robust outcomes. The models were printed with the Photon S (Anycubic, Shenzhen, China) using a 405 nm Resin (Anycubic, Shenzhen, China).

Following the conclusion of the segmentation and having the model in the adequate format, all files have to be imported into a slicing software. This kind of software automatically converts the STL format into specific printing commands usually expressed in G-code. The used slicing softwares were Simplify3D (Cincinatti, Ohio, United States of America) and Cura (Ultimaker, Utrecht, The Netherlands).

2.5 Case studies

The imaging data used in this study has been anonymised following the national regulations of data protection (Regulamento Geral de Proteção de Dados, 2018). The clinical protocols in force at the CRR/CHULC, together with informed consent, data registry and anonymity requirements at hospital level have been validated by the Ethical Committee Board of CHULC.

2.5.1 Case 1 - Kawasaki Disease

The first case is of a paediatric patient with Kawasaki disease (KD). KD is characterised by an inflammation of small to medium arteries that can lead to the formation of coronary aneurysms therefore the coronary arteries are the focal point.

It was decided that the adequate imaging procedure would be a CT due to the great spatial resolution and the greater structure definition ensuring then a superior image quality. In order to assure that the radiation exposure was as low as reasonably achievable, it was administered an iodinated contrast bolus and the imaging was performed at the peak of enhancement in the region of contrast, this case the coronary arteries; this was also combined with low settings of the tube current and kilovoltage.

The CT scan revealed enlarged coronary arteries as expected (figure 3).

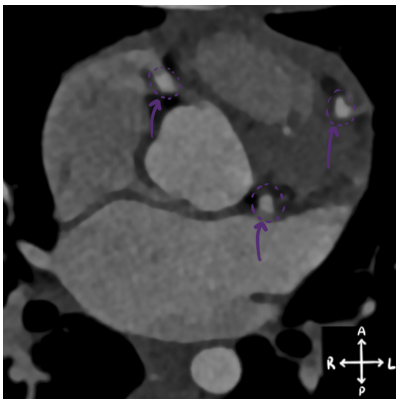

Figure 3: CT scan of the heart of a KD patient. The enlarged coronary arteries are clearly seen (purple circles and arrows). Axial view at the level of the left ventricle outflow.

2.5.2 Case 2 - Tetralogy of Fallot

The second case is of a paediatric patient with a surgically corrected Tetralogy of Fallot (ToF). ToF is usually characterised by four defects: pulmomary valve stenosis (narrowed exit of the right ventricle); ventricular septal defect (hole between the two ventricles); overriding aorta (blood from both ventricles) and right ventricular hypertrophy (thickening of the right ventricle muscle).

Both CT and MRI were performed in this case to combine the CT's significant spatial resolution and structure definition and the MRI's excellent soft tissue distinction and the ability to perform functional studies. With the interest of ensuring the best image quality possible and as low as reasonably achievable radiation exposure, an iodinated contrast bolus and a gadolinium contrast medium were administered in the CT and MRI, respectively.

The CT and MRI scan portrayed a discrepancy on the size of the left and right branch of the pulmonary artery; the right branch is small and short while the left branch has a substantial size (figures 4 and 5).

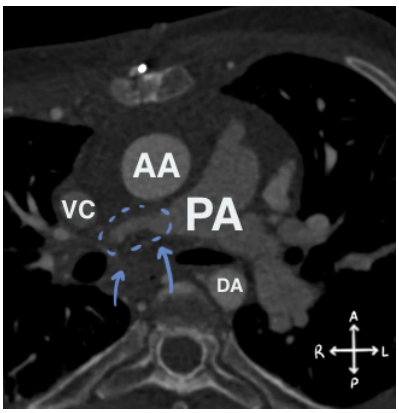

Figure 4: CT scan that shows the disparity in sizes of the left and right branches of the pulmonary artery. The right branch is very small in contrast with the left branch (blue circles and arrows). Axial view.

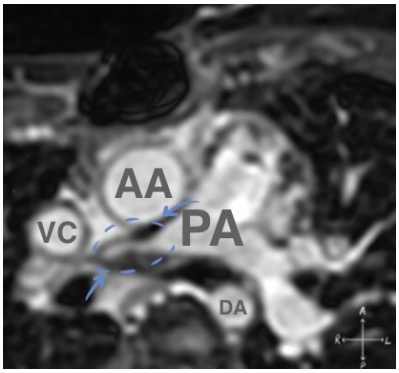

Figure 5: MRI scan that shows the disparity in sizes of the left and right branches of the pulmonary artery. The right branch is very small in contrast with the left branch (blue circles and arrows). Axial view.

In addition, both scans illustrated the surgically corrected pulmonary valve stenosis with presence of grooves on the exit chamber of the right ventricle (figures 4 and 5).

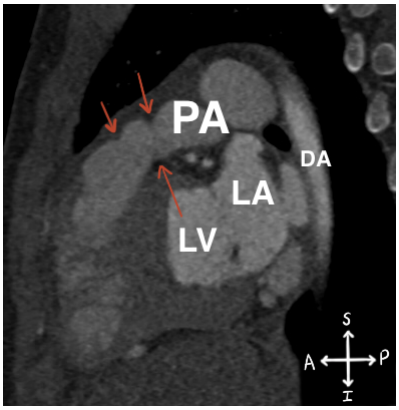

Figure 6: CT scan demonstrates the grooves on the exit chamber of the right ventricle (red arrows). Saggital view.

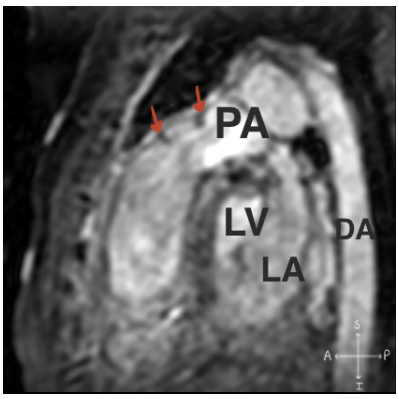

Figure 7: MRI scan illustrates the grooves on the exit chamber of the right ventricle (red arrows). Saggital view.

2.5.3 Case 3 - Complex congenital heart disease

The third case is of a paediatric patient with a surgically corrected complex CHD. This case is characterised by a dextrocardia - where the apex of the heart is located on the right side of the body [16] -, only one atrioventricular valve and, it also has two superior venae cavae (one left and one right) each connected to their respective ipsilateral pulmonary arteries. Only a MRI scan was performed due to the need to perform a functional study on the patient to assess the tissue behaviour post-surgery. Again, the MRI scan was carried out using a gadolinium contrast medium to secure a good distinction between different structures.

The MRI scan showed the presence of two superior venae cavae (SVC), one on the right and one on the left. This becomes visible on the axial and the coronal view (figures 8 and 9).

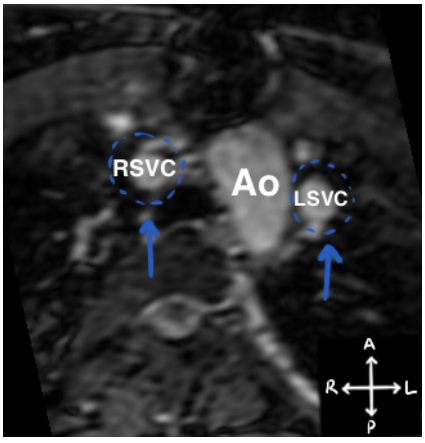

Figure 8: MRI scan of a heart of a patient with complex CHD. It shows the presence of two venae cavae (blue circles and arrows). Axial view.

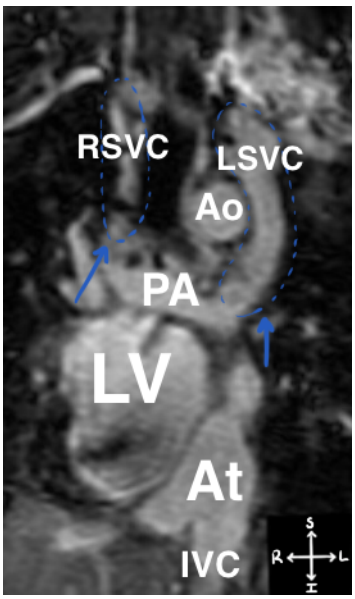

Figure 9: MRI scan of a heart of a patient with complex CHD. It shows the presence of two venae cavae (blue circles and arrows). Coronal view.

Additionally, it corroborates the dextrocardia since the apex points towards the right not the left as usual. Furthermore, it also depicted the only atrioventricular valve present in the heart (figure 10).

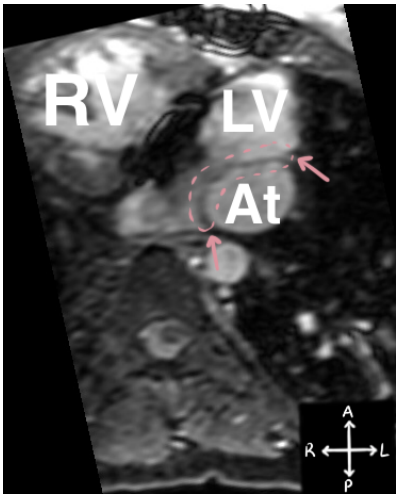

Figure 10: MRI scan of a heart of a patient with complex CHD. It that shows the present dextrocardia (the apex points towards the right) and the only atrioventricular valve (pink circle and arrows). Axial view.

3 Results

3.1 Segment definition

The thresholding method was used to create a 3D rendering of the heart. Since some segments coincided, and there were defects in the segmentation, it was necessary to recur to manual editing so those major flaws could be corrected. Lastly, when all considerable errors were emended, a smoothing effect was applied to produce a smoother outcome and to remove any kind of extrusions or holes.

In order to exemplify the overall results of this thesis, the case where a paediatric patient with a surgically corrected ToF was chosen using the CT data.

Bearing in mind the defects present in this case, the division of left and right heart will suffice to properly illustrate this patient's heart since these defects will be visible.

Thus, there are three segments: right heart, that encompasses the venae cavae, the pulmonary artery, right atria and the right ventricle; left heart, that includes the ascending and descending aorta, the left atria and left ventricle; and soft tissue, that is composed by the cardiac muscle that surrounds the aforementioned structures.

The CT scan of the heart of the patient with ToF had great quality, with a clear distinction between different types of tissues, and sharp definition of structures. There were not any visible artifacts on the scan.

Two types of models were created: one hollow model in which only the soft tissue is present that acts as a visual indicator of the heart's contour and can be used in dosimetric studies (figures 11, 12, 13 and 14); and other model made up by the major internal structures of the heart that serves as a standard for identifying the anomalies present in the structures (figures 15, 16, 17 and 18).

The hollow model was sectioned in two parts according to a transversal plane in order to have physical access to the hollowed parts and for the printing to be easier, as the model has a flat surface, thus reducing the amount of supports printed (figures 12 and 13).

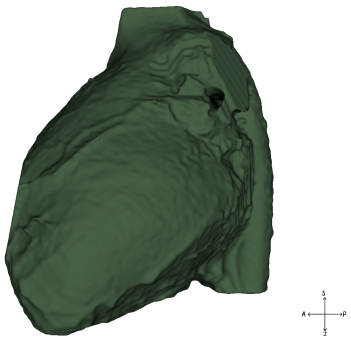

Figure 11: Result of the segmentation made with the CT scan of the heart of the patient with ToF. Left section of the hollow model where the green structure represents the soft tissue. Left view.

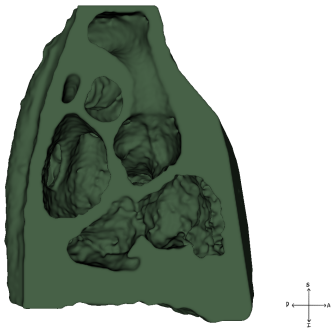

Figure 12: Result of the segmentation made with the CT scan of the heart of the patient with ToF. Left section of the hollow model where the green structure represents the soft tissue. Right view.

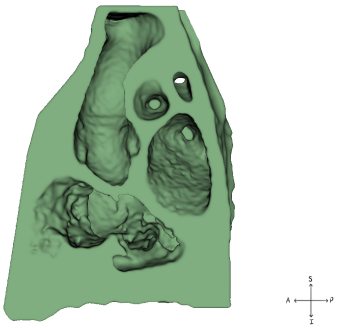

Figure 13: Result of the segmentation made with the CT scan of the heart of the patient with ToF. Right section of the hollow model where the green structure represents the soft tissue. Left view.

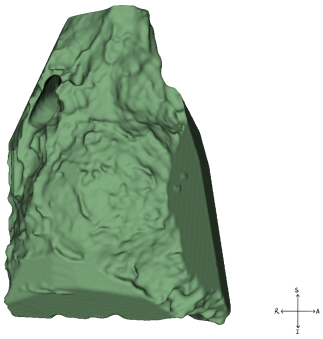

Figure 14: Result of the segmentation made with the CT scan of the heart of the patient with ToF. Right section of the hollow model where the green structure represents the soft tissue. Right view.

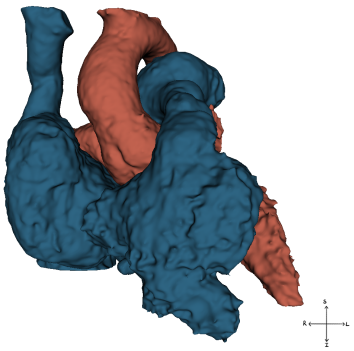

Figure 15: Result of the segmentation made with the CT scan of the heart of the patient with ToF. Blood-pool model where the red illustrates the left heart, and the blue depicts the right heart. Anterior view.

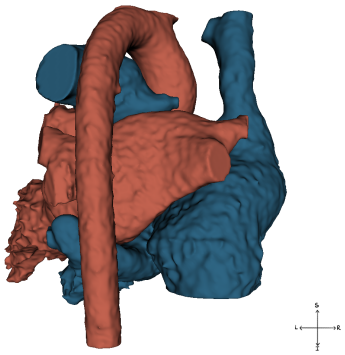

Figure 16: Result of the segmentation made with the CT scan of the heart of the patient with ToF. Blood-pool model where the red illustrates the left heart, and the blue depicts the right heart. Posterior view.

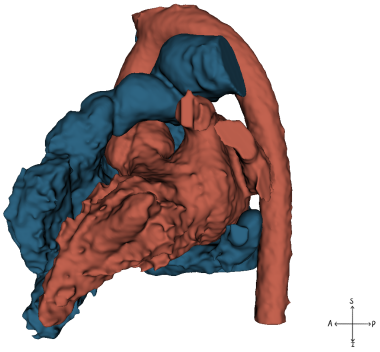

Figure 17: Result of the segmentation made with the CT scan of the heart of the patient with ToF. Blood-pool model where the red illustrates the left heart, and the blue depicts the right heart. Left view.

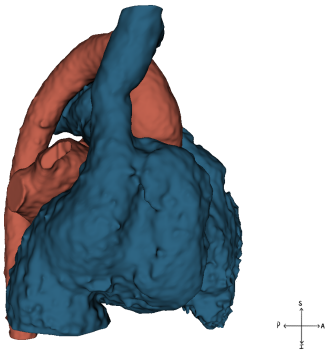

Figure 18: Result of the segmentation made with the CT scan of the heart of the patient with ToF. Blood-pool model where the red illustrates the left heart, and the blue depicts the right heart. Right view.

Some hurdles presented themselves in the segmentation process, such as accurately splitting up structures that were not supposed to be embedded together; trying to distinguish the cardiac tissue from the diaphragm and manually create the inferior part of the enclosure of the heart; deciding whether or not to smooth out the features of the segments to produce a more visually appealing model; and to try to strengthen the structural integrity of the hollow model after the subtraction of the internal structures.

3.1.1 Printed models

Generally, the hollow model had a good printing quality where the outline of the heart is easy to perceive, consequence of the high detail of the CT scan (figures 19, 20, 21 and 22). Furthermore, it is clear that the hollowed parts have quite thorough characteristics result of the subtraction of the internal structures (figure 21).

As a consequence of the intricacies of the hollow model, a large amount of supports were necessary to aid the printing process and for the structural stability of the model. Unfortunately, there were some supports that could not be removed from the model since they were in strange angles, unreachable positions and the lack of adequate tools for removal (figure 20).

Figure 19: Result of the printing of the left section of the hollow model made with the CT scan of the heart of the patient with ToF. Left view.

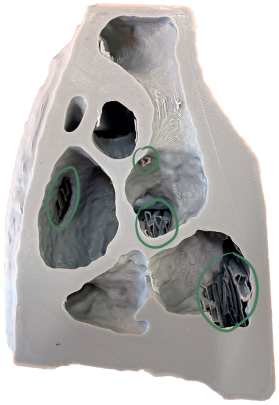

Figure 20: Result of the printing of the left section of the hollow model made with the CT scan of the heart of the patient with ToF. The green circles highlight the supports that could not be removed. Right view.

Figure 21: Result of the printing of the right section of the hollow model made with the CT scan of the heart of the patient with ToF. Left view.

Figure 22: Result of the printing of the right section of the hollow model made with the CT scan of the heart of the patient with ToF. Right view.

The left heart segment had a decent printing quality and presented fine details similar to the ones created in

the segmentation process. While removing some of the supports, a part of the descending aorta fractured from the main model (figures 23 and 24). Considering that the descending aorta was practically supporting itself it came as no surprise when it fractured. One solution to this issue would be to increase the amount of infill on the descending aorta to reinforce the structure.

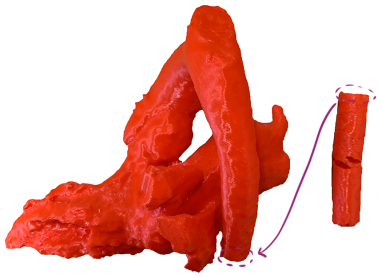

Figure 23: Result of the printing of the left heart segment made with the CT scan of the heart of the patient with ToF. A piece of the descending aorta fractured and, the purple circles and arrow show where the fragment should be. Left view.

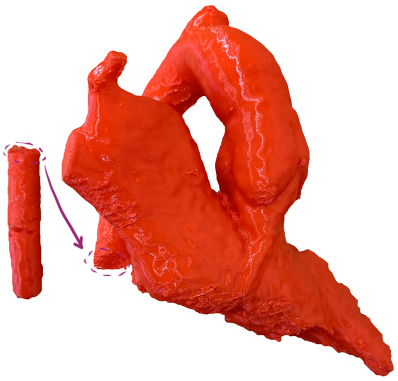

Figure 24: Result of the printing of the left heart segment made with the CT scan of the heart of the patient with ToF. A piece of the descending aorta fractured and, the purple circles and arrow show where the fragment should be. Right view.

The right heart segment also presented a satisfactory printing quality with precise features. Similar to the left heart segment, a piece of the model - the superior vena cava - broke by removal of the supports (figures 25 and 26). Again, if possible, these types of pieces should have more material printed to improve robustness and decrease the likeness of fractures in the model.

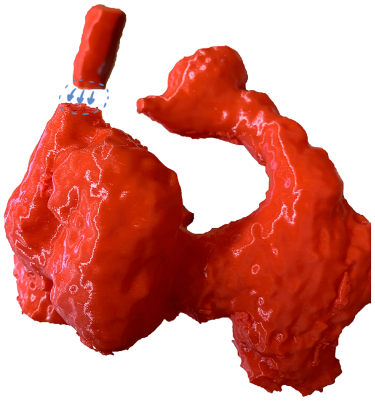

Figure 25: Result of the printing of the right heart segment made with the CT scan of the heart of the patient with ToF. A piece of the superior vena cava fractured and, the blue circle and arrows show where the fragment should be. Anterior view.

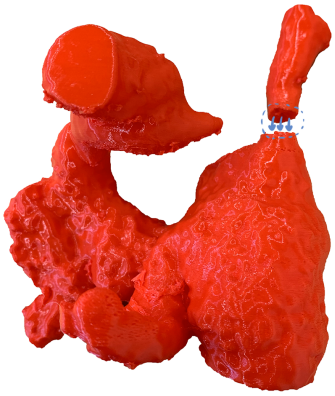

Figure 26: Result of the printing of the right heart segment made with the CT scan of the heart of the patient with ToF. A piece of the superior vena cava fractured and, the blue circle and arrows show where the fragment should be. Posterior view.

3.1.2 Feedback

In regards to the blood-pool models, the physicians emphasised the good quality of segmentation and the precision of anatomical replication. Yet, it was stated that the boundaries of the hollow models were primitive and did not portray correctly the outline of the cardiac tissue. The incorrect shape of certain parts in the hollow models - the flat portions visible in figure 22 - is a segmentation error , effect of the inability to distinguish certain portions of cardiac tissue and other tissues thus having to manually carve out the boundaries of the hollow model.

4 Discussion and Conclusions

Generally speaking, each imaging method has its advantages and disadvantages when it comes to create and print a 3D model based on the data of each scan. A CT

scan has a superior spatial resolution and is a fairly quick, however, it has lower sensitivity and has the increased risk of radiation exposure [17]. A MRI scan has high sensitivity, a good soft tissue contrast, the possibility of performing functional studies and, low risk of radiation exposure, yet, it has a slow scanning speed and it has a high chance of having inevitable artifacts consequence of metallic structures [17]. Bearing this in mind, an adequate equilibrium between these two imaging methods can be met considering they complement each other.

Naturally, this study had several limitations in the segmentation and printing process.

In the segmentation process, differentiating the cardiac tissue from the adjacent tissues emerged as a major issue, more evident on the segmentations that used CT data. Moreover, importing the MRI scans onto the segmentation software turned out a challenge since the most reliable sequences were not recognised in the software, causing interpolation issues and influencing the image quality and the model itself. A way around this matter would be to search and explore different kinds of software that accept these sequences to improve the segmentation quality.

In the printing process, while handling the model and removing some of the supports a few pieces fractured from the main model; a solution to this issue would be to increase the infill density on these fragile spots and if not possible on the whole model therefore increasing the sturdiness of the model but also increasing the printing time. Additionally, removing the supports from the hollow model revealed itself to be a difficult, strenuous and time consuming activity; not all of the supports could be removed.

Despite the fact that the hollow models certainly represent the unique anatomy of each patient, in order to have precise dosimetric measurements that lead to reliable estimations of dose, it is necessary to have models with comparable tissue densities to the cardiac tissue of 1.055 g/mL [18].

Most hollow models in this study were printed with PLA filament due to its low price, resistance to temperature and good mechanical properties [19].

The PLA filament has a density of about 1.25 g/cm^3 and the ABS filament with a density around 1.05 g/cm^3.

At first glance, the ABS filament might seem an excellent candidate to replicate the tissue attenuation. However, and having into account the infill density of the printed models, the overall density of the models decreases for both filaments consequence of the printing parameters, gaps with air, and contractions that might have happened after the cooling of the filament [20].

Therefore, the PLA filament would be the adequate choice for printing the models that accurately replicates the tissue attenuation.

Considering that the ABS filament has measurable hindrances such as the difficulty to maintain proper temperatures and the necessity of a closed printer, all the models can be printed using the PLA filament for an easier printing process.

This thesis proposed to create 3D printed models of the hearts of children with heart disease using images from CT and MRI scans. To do so, the resulting files from the CT and MRI scans were imported into a segmentation software to separate the different regions of the heart and export these segments towards a format compatible with the 3D printer. After this, the files are imported into a slicing software for them to be printed. The final printed models were handled and evaluated by medical doctors.

Upon the analysis of medical doctors, it was concluded that the blood-pool models presented a detailed and meticulous representation of the heart's anatomy and, the hollow models exhibit an off-putting outcome in certain areas as a consequence of drawbacks in the segmentation process. In addition, the models were said to be adequate for surgical planning considering the appropriate representation of the heart's structures, and its role in comprehending, as a whole, the heart conditions.

This work managed to create 3D models that accurately represented the anatomy of hearts of children with heart disease. Furthermore, it accomplished to produce precise hollow models that can be used in dosimetric studies that considers the individual's unique anatomy and that can further aid the search for optimisation of CT parameters with regards to paediatric patients.

5 Future work

Nowadays, the use of 3D printing is limited to procedural planning or simple anatomical teaching. However, with the advances on this technology, the treatment of CHD could encompass patient-specific devices, for instance, homografts, shunts or prosthetic valves such as atrial septal defect (ASD) and ventricular septal defect (VSD) closure valves, and left atrial appendage (LAA) occlusion in order to decrease the frequency of post-procedural device failure and complications given that these devices are suited to each patient's unique anatomy [21].

One of the key elements on developing 3D printed models that can be used in cardiology is the capacity of reproducing with a high degree of accuracy the cardiac tissue and its anatomical properties. Besides, not sectioned hollow models can be used as a teaching tool to simulate interventional cardiology. This will improve the evaluation of the physiological consequences of defects and will better prepare trainees for interventional procedures. With this is mind, it is paramount to realise that using this type of technology to plan complex surgical procedures or to develop custom-made devices demands a highly accurate model of the anatomical properties and minimal errors [21].

In order to achieve these requirements, the 3D printed models have to be printed with more flexible materials that resemble cardiac tissue and its functions. This poses an issue since native cardiac tissue has a lot of intricacies and properties that change over time and physiological state [21].

Additionally, as was previously mentioned, 3D printed models can also be used to obtain dosimetric measurements from ionising radiation procedures and to further advance dose-reduction. So, to secure measurements more accurate as possible, the 3D printed models have to be printed with materials that have similar radiodensities to the different tissues that compose a heart.

Therefore, and due to the novelty of the area of material exploration, research into materials with a wide range

of malleability, than can closely mimic the mechanical and physiological properties of the cardiac tissue, and have resembling radiodensities is crucial and must continue [21]. Moreover, it is imperative that these types of material are affordable so that they do not hinder the progress of using the 3D printing technology in cardiology [1, 2, 5, 21]. Besides the innovative non-biological material research, bioprinting and molecular printing will be key factors in advancing the 3D printing technology. These methods consist on building tissues with complex structures that are biologically engineered thus mimicking cardiac tissue and structures. Yet, these techniques face the issue to create a tissue that is functional and viable [21].

In conclusion, 3D printing has the potential to make a profound transformation in cardiology towards personalised, meticulous and accurate medicine as the 3D printed models can improve the quality of treatment and provide important tools for decision making [21].

References

[1] M. Cantinotti, I. Valverde, S. Kutty, The international journal of cardiovascular imaging **33**, 137 (2017)

[2] S.J. Yoo, O. Thabit, E.K. Kim, H. Ide, D. Yim, A. Dragulescu, M. Seed, L. Grosse-Wortmann, G. van Arsdell, 3D printing in medicine **2**, 3 (2016)

[3] J. Ryan, J. Plasencia, R. Richardson, D. Velez, J.J. Nigro, S. Pophal, D. Frakes, 3D printing in medicine **4**, 10 (2018)

[4] H. Bosmans, J. Damilakis, H.D. le Pointe, S.J. Foley, et al., *European Guidelines on Diagnostic Reference Levels for Paediatric Imaging*, in *Radiation Protection Nº 185* (European Commission, 2018)

[5] M. Vukicevic, B. Mosadegh, J.K. Min, S.H. Little, JACC: Cardiovascular Imaging **10**, 171 (2017)

[6] S. Anwar, G.K. Singh, J. Miller, M. Sharma, P. Manning, J.J. Billadello, P. Eghtesady, P.K. Woodard, JACC: Basic to Translational Science **3**, 294 (2018)

[7] L. Romans, *Computed Tomography for Technologists: A comprehensive text* (Lippincott Williams & Wilkins, 2011)

[8] D.E. Chabner, *Medical terminology: A short course/by davi-ellen chabner* (2015)

[9] X. Zhuang, Journal of healthcare engineering **4**, 371 (2013)

[10] X. Zhuang, Ph.D. thesis, UCL (University College London) (2010)

[11] P. Peng, K. Lekadir, A. Gooya, L. Shao, S.E. Petersen, A.F. Frangi, Magnetic Resonance Materials in Physics, Biology and Medicine **29**, 155 (2016)

[12] S. Pieper, M. Halle, R. Kikinis, *3D Slicer*, in *2004: 2nd IEEE International Symposium on Biomedical Imaging: Nano to Macro (IEEE Cat No. 04EX821)* (2004), pp. 632–635 Vol. 1

[13] X. Zhuang, L. Li, C. Payer, D. Štern, M. Urschler, M.P. Heinrich, J. Oster, C. Wang, Ö. Smedby, C. Bian et al., Medical image analysis **58**, 101537 (2019)

[14] O.S. Carneiro, A. Silva, R. Gomes, Materials & Design **83**, 768 (2015)

[15] S. Corbel, O. Dufaud, T. Roques-Carmes, in *Stereolithography* (Springer, 2011), pp. 141–159

[16] P.D. Maldjian, M. Saric, American Journal of Roentgenology **188**, S39 (2007)

[17] Z. Shaikh, A. Torres, M. Takeoka, Brain Sciences **9**, 190 (2019)

[18] A. Fuchs, M.R. Mejdahl, J.T. Kühl, Z.R. Stisen, E.J.P. Nilsson, L.V. Køber, B.G. Nordestgaard, K.F. Kofoed, European Heart Journal-Cardiovascular Imaging **17**, 1009 (2016)

[19] A. Rodríguez-Panes, J. Claver, A.M. Camacho, Materials **11**, 1333 (2018)

[20] M. Savi, M.A. Andrade, M.P. Potiens, Radiation Physics and Chemistry **174**, 108906 (2020)

[21] M.B. Elshazly, M. Hoosien, in *3D Printing Applications in Cardiovascular Medicine* (Elsevier, 2018), pp. 243–253